J|A|C|S ARTICLES

Published on Web 11/04/2010

# Theoretical Investigation of the Mechanism and Dynamics of Intramolecular Coherent Resonance Energy Transfer in Soft Molecules: A Case Study of Dithia-anthracenophane

Lei Yang,[†] Stefano Caprasecca,[‡] Benedetta Mennucci,[‡] and Seogjoo Jang*,[†]

*Department of Chemistry and Biochemistry, Queens College of the City University of New York, 65-30 Kissena Boulevard, Flushing, New York 11367, United States, and Dipartimento di Chimica e Chimica Industriale, Università di Pisa, via Risorgimento 35, 56126 Pisa, Italy*

Received April 19, 2010; E-mail: seogjoo.jang@qc.cuny.edu

***Abstract:*** A computational study is conducted on dithia-anthracenophane (DTA), for which there is experimental evidence for coherent resonance energy transfer dynamics, and on dimethylanthracene (DMA), a molecule representing the energy donor and the acceptor in DTA. Electronic excitation energies are calculated by configuration interaction singles (CIS) and time-dependent density functional theory (TD-DFT) methods and are compared to experimental ones. Electronic coupling constants are calculated between two DMAs embedded into the ground-state structure of DTA employing methods based on transition densities. The resulting values of electronic coupling provide a more consistent interpretation of experiments than those based on one-half the level spacing of DTA excitation energies. Solvation effects are studied based on the polarizable continuum model (PCM). Solvent-induced polarization and screening effects are shown to make opposite contributions, and the net electronic coupling is little different from the value in a vacuum. The likelihood of coherent population transfer is assessed on the basis of a recently developed theory of coherent resonance energy transfer. The time scale of bath is shown to have an important role in sustaining the quantum coherence. The combination of quantum chemical and dynamical data suggests that the electronic coupling in DTA is in the range of 50−100 $cm^{-1}$. The presence of oscillatory excitation population dynamics can be understood from the picture of polaronic excitation moderately dressed with dispersive vibrational modes. The effect of torsional modulation on the excitation energies of DTA and electronic coupling is examined on the basis of optimized structures with the torsional angle constrained. The result suggests that inelastic effect due to torsional motion cannot be disregarded in DTA.

## I. Introduction

Controlling the migration of electronic excitation energy in systems consisting of soft macromolecules is a critical issue in solar energy conversion,[1−3] sensor development,[4−6] and biomedical imaging.[7,8] To this end, developing a theoretical capability to provide a quantitative and reliable description of excitation energy transfer (EET) or resonance energy transfer (RET) in such systems is crucial. Within rate approaches, well-established theories can be used to determine transfer rate between single chromophores[9−12] or their aggregates.[12−14] However, many molecules being employed for emerging optoelectronic applications exhibit characteristics that go beyond the assumptions of established theories. In particular, recent experimental results suggest quantum coherence may play an important role.[15−23] However, the quantitative effect of quantum coherence on the RET dynamics is not well understood in

[†] Queens College of the City University of New York.
[‡] Università di Pisa.

(1) Coakley, K. M.; McGehee, M. D. *Chem. Mater.* **2004**, *16*, 4533–4542.
(2) Brédas, J.-L.; Norton, J. E.; Cornil, J.; Coropceanu, V. *Acc. Chem. Res.* **2009**, *42*, 1691–1699.
(3) Po, R.; Maggini, M.; Camaioni, N. *J. Phys. Chem. C* **2010**, *114*, 695–706.
(4) Acharya, J. R.; Zhang, H. T.; Li, X.; Nesterov, E. E. *J. Am. Chem. Soc.* **2004**, *131*, 880–881.
(5) Liu, Y.; Ogawa, K.; Schanze, K. S. *J. Photochem. Photobiol., C* **2009**, *10*, 173–190.
(6) Guo, M.; Varnavski, O.; Narayanan, A.; Mongin, O.; Majoral, J.-P.; Blanchard-Desce, M.; Goodson, T., III. *J. Phys. Chem. A* **2009**, *113*, 4763–4771.
(7) Sasaki, K.; Ito, T.; Nishino, N.; Khochbin, S.; Yoshida, M. *Proc. Natl. Acad. Sci. U.S.A.* **2009**, *106*, 16257–16262.
(8) Liu, W.; Greytak, A. B.; Lee, J.; Wong, C. R.; Park, J.; Marshall, L. F.; Jiang, W.; Curtin, P. N.; Ting, A. Y.; Nocera, D. G.; Fukumura, D.; Jain, R. K.; Bawendi, M. G. *J. Am. Chem. Soc.* **2010**, *132*, 472–483.
(9) Förster, Th. *Discuss. Faraday Soc.* **1959**, *27*, 7.
(10) Dexter, D. L. *J. Chem. Phys.* **1953**, *21*, 836–850.
(11) Jang, S.; Jung, Y. J.; Silbey, R. J. *Chem. Phys.* **2002**, *275*, 319–332.
(12) Scholes, G. D. *Annu. Rev. Phys. Chem.* **2003**, *54*, 57.
(13) Jang, S.; Newton, M. D.; Silbey, R. J. *Phys. Rev. Lett.* **2004**, *92*, 218301.
(14) Sumi, H. *J. Phys. Chem. B* **1999**, *103*, 252.
(15) Zhu, F.; Galli, C.; Hochstrasser, R. M. *J. Chem. Phys.* **1993**, *98*, 1042–1057.
(16) Varnavski, O. P.; Ostrowski, J.; Sukhomlinova, L.; Twieg, R. J.; Bazan, G. C.; Goodson, T., III. *J. Am. Chem. Soc.* **2002**, *124*, 1736–1743.
(17) Yamazaki, I.; Akimoto, S.; Yamazaki, T.; Sato, S.; Sakata, Y. *J. Phys. Chem. A* **2002**, *106*, 2122–2128.
(18) Yamazaki, I.; Aratani, N.; Akimoto, S.; Yamazaki, T.; Osuka, A. *J. Am. Chem. Soc.* **2003**, *125*, 7192–7193.
(19) Métivier, R.; Nolde, F.; Müllen, K.; Basché, T. *Phys. Rev. Lett.* **2007**, *98*, 047802.
(20) Engel, G. S.; Calhoun, T. R.; Read, E. L.; Ahn, T.-K.; Mancal, T.; Cheng, Y.-C.; Blankenship, R. E.; Fleming, G. R. *Nature* **2007**, *446*, 782–786.
(21) Collini, E.; Scholes, G. D. *Science* **2009**, *323*, 369–373.

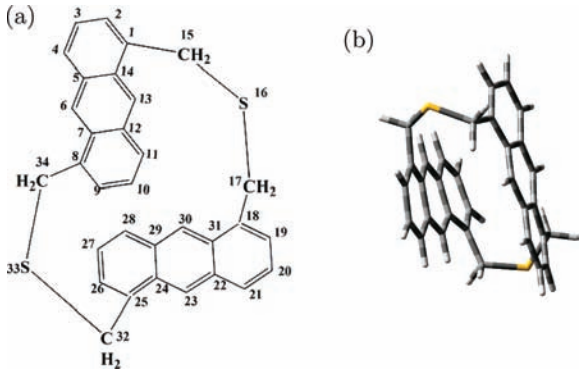


***Figure 1.*** (a) Sketch map of dithia-anthracenophane (DTA) showing labels and atoms. (b) Actual structure of DTA optimized with respect to the ground electronic state.

general. The details of its interplay with molecular and environmental relaxation dynamics also need to be clarified. To cope with these demands, new theoretical approaches have been developed recently.[24−29]

While there are intriguing experimental results in favor of a significant role of quantum coherence,[15−23] direct experimental evidence for the departure of RET dynamics from a rate description due to electronic coherence is difficult to find. In this sense, dithia-anthracenophane (DTA) serves as an important molecular system, for which convincing spectroscopic data for coherent population transfer dynamics are available.[17,30] The molecule also retains key features of soft optoelectronic molecules while being simple enough for detailed computational study. Thus, careful theoretical study of this molecule may reveal qualitative and quantitative details of coherent RET dynamics that are important in soft optoelectronic molecules in general.

DTA is a bichromophoric molecule with two anthracene units linked by covalent bonds via sulfur atoms as shown in Figure 1. According to the X-ray crystallography,[31] the two planes of anthracene units are parallel, and their long axes are almost orthogonal to each other. If the system can be viewed as two excitons localized at anthracene units interacting via transition dipoles, such a structure implies very small electronic coupling. Indeed, Yamazaki et al.[17] found that their experimental estimate of the electronic coupling, 14.5 $cm^{-1}$, is comparable to a theoretical one based on the transition dipole approximation, 20 $cm^{-1}$. Later, another experiment[30] by the same group reported a value of 17.5 $cm^{-1}$. However, considering the proximity of the donor and the acceptor in DTA (3.41 Å according to X-ray data), for which the transition dipole approximation is likely to be inaccurate, this level of agreement is somewhat surprising.

If the value of electronic coupling is indeed small as estimated from experiments, the observation that the RET process in DTA does not fit the rate description[17,30] is another interesting aspect. From a theoretical point of view, this implies that the assumption of Fermi Golden rule, the assumption of incoherent quantum transition,[9−14] does not hold. A theory[32] based on the Bloch−Redfield equation[33] was employed for the analysis of experimental data.[17,30] Similar assumptions were implicit in a recent computational study.[34] However, considering the facts that the time scale of RET dynamics in this molecule is comparable to other molecular time scales and that the system−bath coupling is not necessarily small, it is not clear whether any information based on the Bloch−Redfield type assumptions is quantitatively reliable.

To be more specific, important theoretical issues remain to be answered for DTA. Can the EET dynamics in DTA be understood in terms of the RET process between Frenkel-type excitons[35,36] localized in each anthracene unit? How large is the electronic coupling between the donor and the acceptor? Is the transition dipole approximation valid? How important is the solvation effect? How can coherent RET dynamics persist despite the fact that the electronic coupling is much smaller than intramolecular vibrational relaxation energy? Can there be significant inelastic effects due to the soft nature of the molecule? While there have been impressive theoretical advances in addressing these issues, the efforts in the fields of quantum dynamics[24−29,37] and quantum chemistry[12,38−42] have been rather disjoint so far. We here put these efforts together and attempt to provide a cogent and comprehensive theoretical description of RET process in DTA. Although our analysis in this work is specifically focused on DTA, many issues being addressed and resolved here are relevant to many other soft macromolecular systems. Thus, the present work has much broader implications.

This Article is organized as follows. First, standard computational study is conducted on DTA and its monomer unit. Second, electronic coupling constant is calculated employing the transition density cube (TDC) method[43] and another method[44] based on a perturbative approximation to the time-dependent density functional theory (TD-DFT).[45] Solvation effects are also included within the polarizable continuum model (PCM).[44] Third, a theory of coherent resonance energy transfer (CRET)[25,26] is applied to the model of DTA, and the likelihood and condition for coherent RET dynamics are examined. Finally,

(22) Collini, E.; Wong, C. Y.; Wilk, K. E.; Curmi, P. M. G.; Brumer, P.; Scholes, G. D. *Nature* **2010**, *463*, 644–647.
(23) Gaab, K. M.; Bardeen, C. J. *J. Phys. Chem. B* **2004**, *108*, 4619–4626.
(24) Jang, S. *J. Chem. Phys.* **2007**, *127*, 174710.
(25) Jang, S.; Cheng, Y.-C.; Reichman, D. R.; Eaves, J. D. *J. Chem. Phys.* **2008**, *129*, 101104.
(26) Jang, S. *J. Chem. Phys.* **2009**, *131*, 164101.
(27) Palmieri, B.; Abramvicius, D.; Mukamel, S. *J. Chem. Phys.* **2009**, *130*, 204512.
(28) Ishizaki, A.; Fleming, G. R. *J. Chem. Phys.* **2009**, *130*, 234111.
(29) May, V. *J. Chem. Phys.* **2008**, *129*, 114109.
(30) Sato, S.; Nishimura, Y.; Sakata, Y.; Yamazaki, I. *J. Phys. Chem. A* **2003**, *107*, 10019.
(31) Sakata, Y.; Toyoda, T.; Yamazaki, T.; Yamazaki, I. *Tetrahedron Lett.* **1992**, *33*, 5077–5080.
(32) Wynne, K.; Hochstrasser, R. M. *J. Raman Spectrosc.* **1995**, *26*, 561–569.
(33) Redfield, A. G. *IBM J. Res. Dev.* **1957**, *1*, 19–31.
(34) Kishi, R.; Nakano, M.; Minami, T.; Fukui, H.; Nagai, H.; Yoenda, K.; Takahashi, H. *J. Phys. Chem. A* **2009**, *113*, 5455–5462.
(35) Frenkel, J. *Phys. Rev.* **1931**, *37*, 17–44.
(36) Davydov, A. S. *Theory of Molecular Excitons*; Plenum Press: New York/London, 1971.
(37) Ishizaki, A.; Fleming, G. R. *Proc. Natl. Acad. Sci. U.S.A.* **2009**, *106*, 17255–17260.
(38) Tomasi, J.; Mennucci, B.; Cammi, R. *Chem. Rev.* **2005**, *105*, 2999–3093.
(39) Hsu, C.-P.; Fleming, G. R.; Head-Gordon, M.; Head-Gordon, T. *J. Chem. Phys.* **2001**, *114*, 3065.
(40) Subotnik, J. E.; Cave, R. J.; Steele, P. R.; Shenvi, N. *J. Chem. Phys.* **2009**, *130*, 234102.
(41) Curutchet, C.; Scholes, G. D.; Mennucci, B.; Cammi, R. *J. Phys. Chem. B* **2007**, *111*, 13253.
(42) Gaab, K. M.; Thompson, A. L.; Xu, J.; Martinez, T. J.; Bardeen, C. J. *J. Am. Chem. Soc.* **2003**, *125*, 9288.
(43) Krueger, B. P.; Scholes, G. D.; Fleming, G. R. *J. Phys. Chem. B* **1998**, *102*, 5378–5386.
(44) Iozzi, M. F.; Mennucci, B.; Tomasi, J.; Cammi, R. *J. Chem. Phys.* **2004**, *120*, 7029–7040.
(45) Runge, E.; Gross, E. K. U. *Phys. Rev. Lett.* **1984**, *52*, 997–1000.

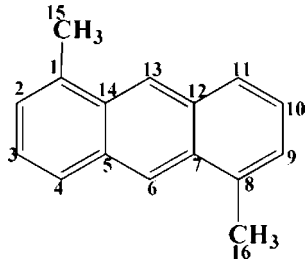


***Figure 2.*** Sketch map of dimethyl anthracene (DMA).

***Table 1.*** Major Bond Distances (Å) and Angles of DMA and DTA in the Ground Electronic State and the Lowest Excited State[a]

| | DMA | | DTA | |
|---|---|---|---|---|
| labels | ground | excited | ground | excited |
| *R*1−2/18−19 | 1.376 | 1.400 | 1.377 | 1.352/1.404 |
| *R*2−3/19−20 | 1.425 | 1.381 | 1.423 | 1.429/1.378 |
| *R*3−4/20−21 | 1.370 | 1.394 | 1.370 | 1.346/1.395 |
| *R*4−5/21−22 | 1.430 | 1.394 | 1.429 | 1.433/1.392 |
| *R*5−6/22−23 | 1.403 | 1.413 | 1.403 | 1.390/1.413 |
| *R*5−14/22−31 | 1.445 | 1.440 | 1.447 | 1.426/1.442 |
| *R*14−13/23−24 | 1.402 | 1.404 | 1.403 | 1.391/1.405 |
| *R*14−1/18−31 | 1.444 | 1.411 | 1.447 | 1.451/1.414 |
| *R*1−15/17−18 | 1.509 | 1.507 | 1.517 | 1.518/1.511 |
| *R*15−16/16−17 | | | 1.851 | 1.827/1.835 |
| $\theta$ (32−33−34) | | | 103.1 | 103.9 |
| $\phi$ (6−13−30−23) | | | 86.06 | 85.94 |

[a] The ground-state structure was optimized by DFT with B3LYP/6-31+G(d,p) level, and the excited state was optimized by CIS/6-31G(d,p). In the column of labels, additional distance labels followed by "/" are shown, which correspond to those for symmetric counter parts in DTA. For the ground electronic state of DTA with $D_2$ symmetry, these two distances are the same. For the excited electronic state of DTA, the two values are different.

the prospect of inelastic effects[24] is assessed on the basis of computational results of constrained optimization.

## II. Electronic Structure Calculation and Optimization

If sulfur atoms in DTA do not make any significant contribution to the electronic coupling in DTA, the dimethylanthracene (DMA) molecule shown in Figure 2 can be perceived as the donor (D) and the acceptor (A) in DTA. To examine this assumption, we conducted a standard computational study of the ground and excited electronic states of both DMA and DTA.

For the geometry optimization of the molecule in the ground electronic state, density functional theory (DFT)[46] was employed with B3LYP functional[47,48] and the basis set 6-31+G(d,p). Solvent effect was not considered. Most of the calculations in this section were performed via the Gaussian 03 package.[49] Table 1 shows the bond distances of optimized DMA and DTA, respectively. In the ground states, the bond lengths in DMA are almost the same as the corresponding ones in DTA. The maximum bond length difference between the two within the anthracene unit is about 0.003 Å. DMA exhibits a planar geometry and belongs to $C_{2h}$ point group in both ground and excited electronic states. On the other hand, DTA has $D_2$ symmetry in the ground electronic state and $C_2$ symmetry in the excited electronic state. In the ground electronic state, the bond angle of the bridge part formed by the sulfur atom is 103.1°. The shorter (or longer) in-plane axes of anthracene units are not orthogonal. The dihedral angle between the two is 86.06°. The distance between the two planes is 3.77 Å, which is somewhat longer than the X-ray structure distance of 3.41 Å that was assumed in other studies.[17,30,34] Considering that DFT/B3LYP cannot account for dispersion interaction properly,[50] this distance appears to overestimate actual distance. We tried optimization of DTA by the second-order Moller−Plesset perturbation theory (MP2) method[51,52] with the same basis set 6-31+G(d,p). The distance between the anthracene units in the resulting structure was 3.19 Å (see the Supporting Information for the structure). Although this may be significant, it is not likely to alter the major conclusion of our work as will be noted at the end of this section.

For the lowest singlet excited states ($S_1$) of DMA and DTA, optimized structures were determined employing configuration interaction singles (CIS)[53] with smaller basis set 6-31G(d,p). Although CIS tends to overestimate the excitation energy, its prediction of excited-state structure is known to be reasonable.[54] The corresponding bond distances are also shown in Table 1. Unlike the ground state, a significant difference can be seen between the lowest excited-state structure of DMA and the corresponding unit in DTA. As expected from the $C_2$ symmetry, the two monomeric units in the excited DTA have different structures as listed in Table 1.

Figure 3 shows the highest occupied molecular orbital (HOMO), the lowest unoccupied molecular orbital (LUMO), HOMO−1, and LUMO+1 for each of DMA and DTA with structure optimized for the ground electronic state. The energies of orbitals are also shown in the unit of $cm^{-1}$. For DMA, all the frontier orbitals exhibit $\pi$ characteristics. It is worth noting that the HOMO shows antibonding characteristics between adjacent benzene subunits, while the LUMO shows bonding characteristics. This is consistent with the decrease of corresponding inter-ring bond lengths in the excited states that are listed in Table 1. As will be shown in Table 2, the major component of the lowest singlet excited state corresponds to the excitation from the HOMO to the LUMO. Thus, the differences of bond lengths between the ground ($S_0$) and the lowest singlet excited state ($S_1$), which are shown in Table 1, can be understood from the nodal patterns of HOMO/LUMO. For example, the HOMO orbital has nodes between bonds C2−C3, C4−C5, C5−C14, C14−C1, whereas the LUMO orbital has bonding characteristics in these regions. This explains the contraction of these inter-ring bond lengths upon excitation. On the other hand, the HOMO orbital has bonding characteristics with respect to bonds C1−C2, C3−C4, C5−C6, C6−C7, C12−C13, C13−C14, while the LUMO orbital has nodes in these regions. The data in Table 1 indicate that these bond lengths become elongated in the excited state.

For DTA, the situation is more complicated. The bond lengths of excited DTA cannot be explained based on the feature of a single MO. Both the HOMO−1 and the HOMO of DTA

(46) Kohn, W.; Sham, L. J. *Phys. Rev.* **1965**, *140*, A1133–A1138.
(47) Becke, A. D. *J. Chem. Phys.* **1993**, *98*, 5648–5652.
(48) Stephens, P. J.; Devlin, J. F.; Chabalowski, J. F.; Frisch, C. F. *J. Phys. Chem.* **1994**, *98*, 11623–11627.
(49) Frisch, M. J.; et al. *Gaussian 03*, revision D.1; Gaussian, Inc.: Wallingford, CT, 2005.
(50) Sinnokrot, M. O.; Sherrill, C. D. *J. Phys. Chem. A* **2006**, *110*, 10656–10668.
(51) Mller, C.; Presset, M. S. *Phys. Rev.* **1934**, *46*, 618–622.
(52) Head-Gordon, M.; Pople, J. A.; Frisch, M. J. *Chem. Phys. Lett.* **1988**, *153*, 503–506.
(53) Foresman, J. B.; Head-Gordon, M.; Pople, J. A.; Frisch, M. J. *J. Phys. Chem.* **1992**, *96*, 135–149.
(54) Gierschner, J.; Cornil, J.; Egelhaaf, H.-J. *Adv. Mater.* **2007**, *19*, 173–191.

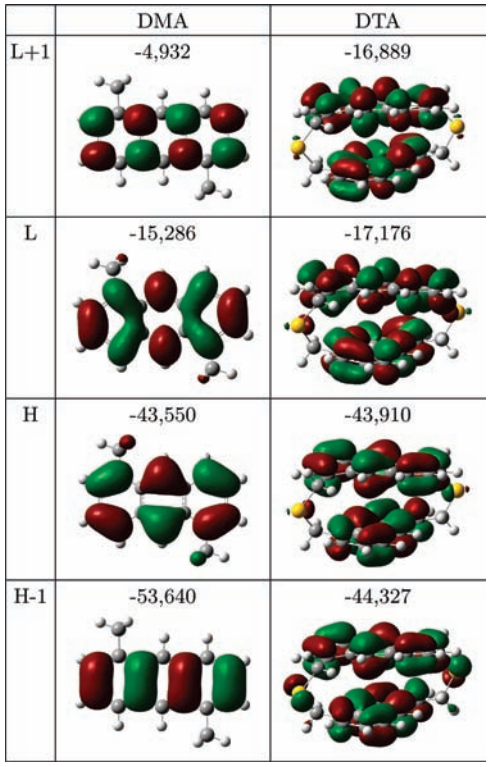


***Figure 3.*** Frontier molecular orbitals of DMA and DTA with structures optimized for respective ground electronic states. "L" represents LUMO, and "H" represents HOMO. Energies of orbitals are shown in the unit of $cm^{-1}$.

correspond to linear combinations of the two equivalent HOMOs of the anthracene units. Likewise, the LUMO and LUMO+1 of DTA originate from the two equivalent LUMOs of the anthracene units. This view is also consistent with the orbitals and energies of DTA shown in Figure 3. Thus, there are four possible elementary transitions with similar energies as follows: HOMO−1 → LUMO, HOMO → LUMO, HOMO−1 → LUMO+1, and HOMO → LUMO+1. Actual transitions can be linear combinations of some of these.

For each molecule, excitation energies were calculated by the TD-DFT method for both structures optimized with respect to the ground ($S_0$) and the lowest singlet excited state ($S_1$). The B3LYP functional[47,48] and 6-31+G(d,p) basis were used. Table 2 provides the transition energies, oscillator strengths, and main configurations for the most relevant singlet excited states. (Results for 6-31G(d,p) are similar. See the Supporting Information.)

According to Yamazaki et al.,[17] the maximum of DTA absorption spectrum is at about 26 320 $cm^{-1}$. This is comparable to the TD-DFT value of $S_0 \rightarrow S_1$ frequency of 25 525 $cm^{-1}$ for a DMA with its structure optimized for the ground electronic state. On the other hand, the maximum of the transient fluorescence spectrum taken during 0−25 ps is at about 23 000 $cm^{-1}$. This is comparable to the TD-DFT value of $S_1 \rightarrow S_0$ emission frequency 22 790 $cm^{-1}$, for the DMA optimized with respect to the $S_1$ state. The CIS method with 6-31G(d,p) basis was used for this excited-state optimization. These calculation results are consistent with the view[17] that the experimental absorption and the transient fluorescence spectra of DTA are characteristic of DMA.

On the other hand, the peak maximum of the stationary fluorescence spectrum (after 50 ps) is more red-shifted[17] than the transient one and occurs around 21 322 $cm^{-1}$. This is comparable to the TD-DFT value of the $S_1 \rightarrow S_0$ emission frequency 21 076 $cm^{-1}$ of DTA with its structure optimized for the $S_1$ state by the CIS method. The $D_2$ symmetry is broken in this excited state as observed in a similar molecular system.[55]

According to the assignments given above, the 408 nm pump pulse (24 510 $cm^{-1}$) in Yamazaki et al.'s experiment[17] matches the TD-DFT excitation energies to the $S_3$ and $S_4$ states of DTA, 23 956 and 24 243 $cm^{-1}$, which have major oscillator strengths. Figure 4 compares the transition density for the $S_0 \rightarrow S_1$ excitation of DMA with those for $S_0 \rightarrow S_3$ and $S_0 \rightarrow S_4$ excitations of DTA. The latter two appear to be symmetric and antisymmetric linear combinations of two $S_0 \rightarrow S_1$ transitions of DMA except for small through-bond contributions via sulfur atoms. Thus, qualitatively, $S_3$ and $S_4$ states of TD-DFT calculation can be viewed as symmetric and antisymmetric Frenkel excitons formed by the $S_1$ excitons of the two anthracene units.

It is known that TD-DFT often underestimates the excitation energy of delocalized excited states or results in unphysical low-lying excited states.[56,57] The presence of two dark singlet states $S_1$ and $S_2$, for the structure optimized for its ground electronic state, may indeed be an example of such artifact. To check this, an additional CIS calculation was conducted to calculate excitation energies for the same ground-state structure of DTA. The results are shown in Table 2. While the excitation energies are substantially higher than experimental ones, the two lowest excited states ($S_1$ and $S_2$) in this calculation have the major oscillator strengths. Their transition densities are similar to those of $S_3$ and $S_4$ obtained from the TD-DFT calculation as well (see the Supporting Information). If we accept that the CIS calculation results are qualitatively correct, the presence of low-lying dark singlet states predicted from the TD-DFT calculation may not be a reality. For further examination of this issue, comparison with higher level calculations[57,55] is needed.

To examine the contribution of sulfur bonds and effects of structural change, we performed calculations for dimers of DMA prepared in two different ways. The first one (I) was taken from the structure of DTA optimized with respect to its ground electronic state by removing sulfur atoms and adding an hydrogen atom to each methylene unit. Additional optimization was made for the four added hydrogen atoms. The second one (II) was constructed by embedding two identical DMAs into the configuration of DTA so that the coordinates of three atoms in each anthracene unit match. The structure of DMA being embedded here was obtained so that the bond distances in Table 1 are constrained to the average values of those for the ground and excited electronic states while all others are optimized. Figure 5 shows the side structures of the two $(DMA)_2$'s in comparison with DTA. Table 3 provides the data for the four lowest singlet electronic transitions.

Comparison of the data for $(DMA)_2$,I in Table 3 to those for DTA in Table 2 shows that the replacement of sulfur bonds with hydrogen atoms increases transition energies by about 400 $cm^{-1}$. In comparison, the relative differences in energy between $S_3$ and $S_4$ states are much less sensitive to the change. This shows that the contribution of through-bond interaction to

(55) Fink, R. F.; Seibt, J.; Engel, V.; Renz, M.; Kaupp, M.; Lochbrunner, S.; Mei Zhao, H.; Pfister, J.; Würthner, F.; Engels, B. *J. Am. Chem. Soc.* **2008**, *130*, 12858–12859.
(56) Dreuw, A.; Head-Gordon, M. *Chem. Rev.* **2005**, *105*, 4009–4037.
(57) Fink, R. F.; Pfister, J.; Zhao, H. M.; Engels, B. *Chem. Phys.* **2008**, *346*, 275–285.

***Table 2.*** Excitation Energies (in $cm^{-1}$) for Two Singlet Transitions of DMA and Four Singlet Transitions of DTA[a]

| molecule | structure | method | transition | $cm^{-1}$ | *f* | CI main coefficients |
|---|---|---|---|---|---|---|
| DMA | I | TD-B3LYP/6-31+G(d,p)//B3LYP/6-31+G(d,p) | $S_0 \rightarrow S_1$ | 25 525 | 0.0792 | H-1 → L+1, −0.12039; H → L, 0.63975 |
| | | | $S_0 \rightarrow S_2$ | 30 858 | 0.0000 | H-1 → L, 0.50930; H → L+1, 0.51091 |
| | II | TD-B3LYP/6-31+G(d,p)//CIS/6-31G(d,p) | $S_0 \rightarrow S_1$ | 22 790 | 0.0831 | H-1 → L+1, −0.10853; H → L, 0.62724 |
| | | | $S_0 \rightarrow S_2$ | 30 231 | 0.0005 | H-1 → L, 0.50270; H → L+1, 0.51833 |
| DTA | I | TD-B3LYP/6-31+G(d,p)//B3LYP/6-31+G(d,p) | $S_0 \rightarrow S_1$ | 22 386 | 0.0043 | H-1 → L+1, 0.41314; H → L, 0.57094 |
| | | | $S_0 \rightarrow S_2$ | 22 482 | 0.0012 | H-1 → L, 0.48032; H → L+1, 0.51623 |
| | | | $S_0 \rightarrow S_3$ | 23 956 | 0.0286 | H-1 → L, 0.47676; H → L+1, −0.43376 |
| | | | $S_0 \rightarrow S_4$ | 24 243 | 0.0516 | H-1 → L+1, 0.53446; H → L, −0.35911 |
| | | CIS/6-31+G(d,p)//B3LYP/6-31+G(d,p) | $S_0 \rightarrow S_1$ | 31 291 | 0.0718 | H-1 → L, −0.42450; H → L+1, 0.48425 |
| | | | $S_0 \rightarrow S_2$ | 31 731 | 0.1424 | H-1 → L+1, −0.43313; H → L, 0.47522 |
| | | | $S_0 \rightarrow S_3$ | 36 245 | 0.0002 | H-3 → L, 0.31300; H-2 → L+1, −0.33540 |
| | | | $S_0 \rightarrow S_4$ | 36 540 | 0.0002 | H-3 → L+1, −0.33422; H-2 → L, 0.33303 |
| | II | TD-B3LYP/6-31+G(d,p)//CIS/6-31G(d,p) | $S_0 \rightarrow S_1$ | 21 076 | 0.0338 | H-1 → L, 0.33672; H → L, 0.55751 |
| | | | $S_0 \rightarrow S_2$ | 21 446 | 0.0151 | H-1 → L, 0.62012; H → L, −0.29197 |
| | | | $S_0 \rightarrow S_3$ | 21 975 | 0.0005 | H → L+1, 0.70427 |
| | | | $S_0 \rightarrow S_4$ | 25 661 | 0.0364 | H-1 → L+1, 0.64743 |
| | | CIS/6-31G(d,p)//CIS/6-31G(d,p) | $S_0 \rightarrow S_1$ | 28 179 | 0.1487 | H → L, 0.66869 |
| | | | $S_0 \rightarrow S_2$ | 34 591 | 0.0897 | H-1 → L+1, 0.63246 |
| | | | $S_0 \rightarrow S_3$ | 35 416 | 0.0013 | H-3 → L, 0.46744; H → L+2, −0.35488 |
| | | | $S_0 \rightarrow S_4$ | 38 717 | 0.0031 | H-2 → L+1, 0.47153; H-1 → L+2, −0.35098 |

[a] The oscillator strength *f* and CI main coefficients of each transition are shown. For each molecule, structure I represents the one optimized for the ground electronic state by the DFT calculation. Structure II represents the one optimized for the lowest singlet excited state by the CIS calculation.

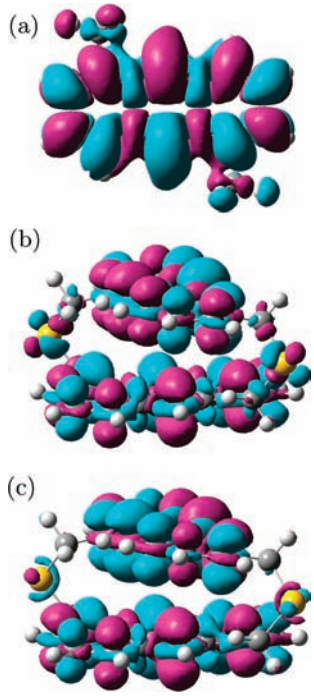


***Figure 4.*** Transition densities for the excitations calculated by TD-DFT with the B3LYP functional. (a) $S_0 \rightarrow S_1$ transition for DMA optimized for ground electronic state. (b) $S_0 \rightarrow S_3$ transition for DTA optimized for the ground electronic state. (c) $S_0 \rightarrow S_4$ transition for DTA optimized for the ground electronic state.

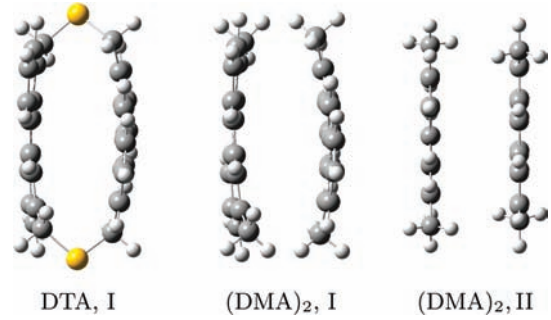


***Figure 5.*** Side views of DTA,I (in Table 2), $(DMA)_2$,I, and $(DMA)_2$,II (in Table 3).

the electronic coupling between the two anthracene units is relatively minor. For structure II of $(DMA)_2$, Table 3 shows that the excitation energy for the $S_3$ increases by about 100 $cm^{-1}$, while that for $S_4$ decreases slightly.

Within an effective two-state picture and for symmetric structure, the electronic coupling between two diabatic states is equal to one-half the level spacing.[58] From TD-DFT excitation energies in Tables 2 and 3, these values were calculated for the three structures shown in Figure 5. The results are presented in Table 4. The electronic coupling in DTA, 144 $cm^{-1}$, is larger than 125 $cm^{-1}$ for $(DMA)_2$,I and much larger than 44.4 $cm^{-1}$ for $(DMA)_2$,II. The comparison between the first two indicates that the contribution through sulfur bonds to the electronic coupling is about 80 $cm^{-1}$. On the other hand, the difference between $(DMA)_2$,I and $(DMA)_2$,II of about 80 $cm^{-1}$ is rather substantial.

To gain better understanding of physical implications of these values, we tried a different functional, M06-2X, a meta functional developed by Zhao and Truhlar.[59] The Gaussian 09 package[60] was used for these calculations. Because we are interested in the effects of different functionals on TD-DFT calculation only, the same structures were used. Table 3 provides excitation energies calculated for the two dimers. The excitation energies are much higher than the experimental values. (This remains the same even when a structure optimized by the M06-2X functional is used. See the Supporting Information.) However, the order of excitation energies seems to be in the right trend. As in the case of CIS calculation, the two lowest excited states are bright. Thus, the difference between $S_0 \rightarrow S_1$ and $S_0 \rightarrow S_2$ was used to estimate the electronic coupling. The resulting values are shown in Table 4 along with others. It is interesting to see that the electronic coupling for $(DMA)_2$,I is

(58) Hsu, C.-P. *Acc. Chem. Res.* **2009**, *42*, 509–518.

(59) Zhao, Y.; Truhlar, D. G. *Theor. Chem. Acc.* **2007**, *120*, 215–241.
(60) Frisch, M. J.; et al. *Gaussian 09*, revision A.1; Gaussian, Inc.: Wallingford, CT, 2009.

***Table 3.*** Excitation Energies (in $cm^{-1}$) for Four Lowest Singlet Transitions of the Dimer of DMA Separated by a Distance of 3.77 Å[a]

| molecule and structure | method | transition | $cm^{-1}$ | $f$ | CI main coefficients |
|---|---|---|---|---|---|
| $(DMA)_2$,I | TD-B3LYP/6-31+G(d,p)//B3LYP/6-31+G(d,p) | $S_0 \rightarrow S_1$ | 22 610 | 0.0035 | H-1 → L+1, −0.38274; H → L, 0.59022 |
| | | $S_0 \rightarrow S_2$ | 22 722 | 0.0002 | H-1 → L, −0.43258; H → L+1, 0.55573 |
| | | $S_0 \rightarrow S_3$ | 24 376 | 0.0311 | H-1 → L, 0.51890; H → L+1, 0.38113 |
| | | $S_0 \rightarrow S_4$ | 24 625 | 0.0408 | H-1 → L+1, 0.55531; H → L, 0.32553 |
| | TD-M06-2X/6-31+G(d,p)//B3LYP/6-31+G(d,p) | $S_0 \rightarrow S_1$ | 27 046 | 0.033 | H-1 → L, −0.3837; H → L+1, 0.58748 |
| | | $S_0 \rightarrow S_2$ | 27 291 | 0.0595 | H-1 → L+1, −0.39046; H → L, 0.58282 |
| | | $S_0 \rightarrow S_3$ | 29 466 | 0.0015 | H-1 → L+1, 0.57413; H → L, 0.37961 |
| | | $S_0 \rightarrow S_4$ | 29 645 | 0.0115 | H-1 → L, 0.58814; H → L+1, 0.38788 |
| $(DMA)_2$,II | TD-B3LYP/6-31+G(d,p)//B3LYP/6-31+G(d,p) | $S_0 \rightarrow S_1$ | 22 394 | 0.0002 | H-1 → L+1, −0.33813; H → L, 0.61247 |
| | | $S_0 \rightarrow S_2$ | 22 488 | 0.0046 | H-1 → L, −0.39284; H → L+1, 0.58427 |
| | | $S_0 \rightarrow S_3$ | 24 510 | 0.0195 | H-1 → L+1, 0.58389; H → L, 0.27882 |
| | | $S_0 \rightarrow S_4$ | 24 599 | 0.0611 | H-1 → L, 0.54607; H → L+1, 0.54607 |
| | TD-M06-2X/6-31+G(d,p)//B3LYP/6-31+G(d,p) | $S_0 \rightarrow S_1$ | 26 609 | 0.0175 | H-1 → L+1, −0.32500; H → L, 0.62322 |
| | | $S_0 \rightarrow S_2$ | 27 035 | 0.0889 | H-1 → L, −0.40187; H → L+1, 0.57443 |
| | | $S_0 \rightarrow S_3$ | 29 200 | 0.0013 | H-1 → L, 0.56636; H → L+1, 0.39180 |
| | | $S_0 \rightarrow S_4$ | 29 496 | 0.0096 | H-1 → L+1, 0.62333; H → L, 0.32742 |

[a] Structure I was obtained from the structure of DTA by removing sulfur atoms and adding hydrogen atoms to the methylene units and then optimizing the additional hydrogen atoms. Structure II was obtained by averaging the distance of DMA's ground and excited states and embedding them into configuration of DTA so that the distance and orientation of them are the same as those in DTA.

***Table 4.*** Total Electronic Couplings (in $cm^{-1}$) Estimated from One-Half the Level Spacings of TD-DFT Excitation Energies in Tables 2 and 3[a]

| DTA,I | $(DMA)_2$,I | | $(DMA)_2$,II | | $(DMA)_2$,II′ | |
|---|---|---|---|---|---|---|
| B3LYP | B3LYP | M06-2X | B3LYP | M06-2X | $V_{TDC}$ | $V_{dp}$ |
| 144 | 125 | 123 | 44.4 | 213 | 51.7 | 231 |

[a] For B3LYP, $\delta E_{43}/2$ is used. For M06-2X, $\delta E_{21}/2$ is used. Coulomb couplings based on both TDC and transition dipole approximation are also shown between DMAs arranged in the same way as $(DMA)_2$,II, except that one has excited structure and the other has ground-state structure. This is denoted as $(DMA)_2$,II′. All the values here are for a vacuum.

insensitive to the choice of functional. However, the value for $(DMA)_2$,II is not. In particular, the value of 213 $cm^{-1}$ seems unreliable. Thus, for this structure, errors associated with functionals appear to make a significant contribution.

As noted earlier in this section, the distance between anthracene units in DTA can be shorter according to the MP2 calculation. Therefore, it is worthwhile to mention the effect of shorter distance between anthracene units. To examine this issue, we tried similar calculations for a different structure of DTA optimized by DFT-M06-2X/6-31+G(d,p), for which the distance is between those obtained from MP2 and DFT/B3LYP. The resulting estimates for electronic couplings based on level spacings of TD-DFT excitation energies (see the Supporting Information) are 96.5 $cm^{-1}$ for DTA and 98.5 $cm^{-1}$ for $(DMA)_2$,I. Thus, the shorter distance does not necessarily make the coupling larger. Rather, the change is more subtle and is within the error range of values obtained for DFT/B3LYP structure.

## III. Resonance Energy Transfer

**A. Coulomb Coupling between DMAs by Transition Density Cube (TDC) Method.** The Coulomb coupling was calculated for two DMAs arranged as in the structure of $(DMA)_2$,II, but one in its first excited-state structure and the other in the ground-state structure. This structure is termed II′. The transition density cube (TDC) method developed by Krueger et al.[43] was used. The TDC method is a method to calculate the Coulomb coupling, which is exact within the Frenkel exciton theory except for approximation involved in the finite size of the cube density element. A brief summary of the TDC method is provided below.

First, electronic structure calculation is conducted to determine wave functions of the initial (i) and final (f) electronic states of molecule α. The transition density of α is defined by

$$\rho_\alpha^{i\rightarrow f}(x,y,z) = \Psi_{\alpha i}(x,y,z)\Psi^*_{\alpha f}(x,y,z) \quad (1)$$

where $\Psi_{\alpha i}$ and $\Psi_{\alpha f}$ represent the wave functions of the initial and final electronic states, respectively.

Second, the integration of the density within a cube element $j$, denoted as $M_\alpha^{g\rightarrow e}(j)$, is approximated with the transition cube element generated from the G03 package as follows:

$$M_\alpha^{g\rightarrow e}(j) = \rho_\alpha^{g\rightarrow e}(x_j,y_j,z_j)\delta_x\delta_y\delta_z \quad (2)$$

where $x_j$, $y_j$, and $z_j$ are coordinates of the $j$th cube, and $\delta_x$, $\delta_y$, and $\delta_z$ are lengths of the cube along respective Cartesian directions. Thus, the volume of the cube is equal to $V_\delta = \delta_x\delta_y\delta_z$.

Finally, the Coulomb coupling between D and A is computed according to

$$V_{TDC} \cong \sum_{jk} \frac{M_D^{e\rightarrow g}(j)M_A^{g\rightarrow e}(k)}{r_{jk}} \quad (3)$$

where $M_D^{e\rightarrow g}(j)$ and $M_A^{g\rightarrow e}(k)$ are transition cube elements of D and A, and $r_{jk}$ is their separation.

TDC calculation was conducted for $(DMA)_2$,II′ by using the transition cube elements for $S_0 \rightarrow S_1$ excitation for each of the ground and excited state DMAs. The TD-DFT method was used with the B3LYP functional and 6-31+G(d,p) basis. The center-to-center distance between the two DMAs is 3.77 Å, and the angle (not dihedral angle) between the two short axes of anthracene units is 93.4°.

As is clear from the transition density in Figure 4a, the direction of the transition vector is not parallel to the short axis of the anthracene unit but is rotated toward the methyl side groups. The senses of this rotation in the two anthracene units are opposite to each other. As a result, the transition dipole interaction is nonzero even when the axes of DMAs become perpendicular to each other.

The number of cube elements for the transition densities used was 512 000. The resulting transition dipole had the same orientation as the one in the Gaussian output file, but the magnitude of the former was larger than that of the latter by

***Table 5.*** Coulomb Couplings (in $cm^{-1}$) between DMAs at Different Distances Calculated by TDC Method and Dipole Approximation[a]

| $R$ (Å) | $V_{TDC}$ | $V_{dp}$ |
|---|---|---|
| 3.77 | 51.7 | 231 |
| 5.00 | 36.4 | 98.9 |
| 10.0 | 9.04 | 12.4 |
| 20.0 | 1.42 | 1.55 |

[a] Orientational factor of 0.344 remains the same.

about a factor of 1.41. A scaling factor within the TDC program was used so that the theoretical value of oscillator strength of DMA is reproduced. When tested for a larger number of cube elements, the convergence of the scaled value was reasonable.

The result is shown in Table 4 and compared to the estimates of the total electronic coupling calculated from the level spacings of TD-DFT excitation energies. The calculated value of Coulomb coupling, 51.7 $cm^{-1}$, is very close to the estimate of 44.4 $cm^{-1}$ from the level spacing. However, considering the large discrepancy between this value and that estimated from M06-2X functional calculation, such agreement appears to be fortuitous.

To test the reliability of the transition dipole approximation, we calculated the following transition dipole interaction:

$$V_{dp} = \frac{\kappa|\boldsymbol{\mu}_D||\boldsymbol{\mu}_A|}{R^3} \tag{4}$$

where $\boldsymbol{\mu}_D$ and $\boldsymbol{\mu}_A$ are transition dipole vectors of the donor DMA and the acceptor DMA, respectively. $R$ is the distance between them, and $\kappa$ is the orientational factor defined as

$$\kappa = \hat{\boldsymbol{\mu}}_D \cdot \hat{\boldsymbol{\mu}}_A - 3(\hat{\boldsymbol{\mu}}_D \cdot \hat{\mathbf{R}})(\hat{\boldsymbol{\mu}}_A \cdot \hat{\mathbf{R}}) \tag{5}$$

where $\hat{\boldsymbol{\mu}}_D$, $\hat{\boldsymbol{\mu}}_A$, and $\hat{\boldsymbol{R}}$ are unit transition dipole and distance vectors. As stated earlier in this Article, $R = 3.77$ Å. The value of orientational factor $\kappa = 0.344$ was obtained from the TDC program. The magnitudes of transition dipoles are $|\boldsymbol{\mu}_D| = 2.764$ Debye (D) and $|\boldsymbol{\mu}_A| = 2.557$ D. The resulting value of transition dipole interaction is 231 $cm^{-1}$, which is more than a factor of 4 larger than the TDC value. Thus, it is clear that the dipole approximation is unreliable.

To check the convergence of Coulomb coupling in the large distance limit, calculation of both TDC and transition dipole couplings was made with increasing distance between the two DMAs starting from the structure II. The values in Table 5 confirm that a reasonable convergence is reached at much larger distance around 20 Å. This result is also consistent with another computational study.[61]

For comparison with experimental results, solvation effects need to be accounted for. If we assume that the effective optical dielectric constant is the same as the bulk value of tetrahydrofuran (THF), $\varepsilon_{opt} = 1.98$, the resulting Coulomb coupling including the screening effect in simple treatment[62] is equal to its value in a vacuum divided by $n^2 = \varepsilon_{opt}$. Thus, from the TDC value, it becomes 26.3 $cm^{-1}$. This is comparable to but somewhat larger than the experimental estimates,[17,30] 14.5 and 17.5 $cm^{-1}$. However, this estimate does not include the local field effect. A more satisfactory treatment is presented in the following subsection.

**B. Solvation Effect within Polarizable Continuum Model (PCM).** In the present subsection, the electronic coupling between two DMAs is calculated including the solvation effects within the polarizable continuum model (PCM) implemented by an integral equation formalism (IEF).[38] In this IEFPCM model, the molecular system of the D and A pair (solute) is described at a quantum mechanical level, while the environment is described as a structureless polarizable continuum, characterized by its macroscopic dielectric permittivity. The polarization induced by the solute on the environment is represented in terms of a set of apparent charges placed on the surface of the molecular cavity containing the solute. Such a cavity is modeled on the real structure of the solute using a three-dimensional envelope of atom-centered spheres. The reaction field due to the apparent surface charges is introduced into the quantum mechanical Hamiltonian of the solute, and the resulting nonlinear problem is solved self-consistently. In this way, a mutually polarized solute−environment system is obtained, which accounts for the effects of realistic molecular shape and reaction field of solvent upon solute.

Frenkel exciton theory is assumed in calculating the electronic coupling constant. Thus, perturbation theory is employed within the TD-DFT approach,[39] where the effective electronic coupling is calculated as a perturbation term with respect to interaction-free D and A excitations. In implementing the IEFPCM, a nonequilibrium polarization is introduced in response to these electronic excitations. The changes in the apparent charges representing the response of the solvent are determined by the optical dielectric constant ($\varepsilon_{opt}$) instead of the static one ($\varepsilon_0$). All the calculations in this subsection were made by a locally modified version of G09 package.[60]

The electronic coupling consists of two terms. The first term is calculated from the direct interaction of the transition densities of D and A, each immersed in a polarizable continuum.[44] This is termed solute coupling, $V_s$, which includes the effects of the environment implicitly in the values of the transition densities. In addition, there is an explicit contribution due to the solvent response, $V_{expl}$, which accounts for the screening effects. The total electronic coupling is given by the sum of the two as follows:

$$V = V_s(\rho_D^T, \rho_A^T) + V_{expl}(\Phi_{RF}(\varepsilon_{opt};\rho_D^T), \rho_A^T) \tag{6}$$

where $\rho_D^T$ and $\rho_A^T$ indicate the transition densities of the donor and acceptor molecules, respectively, and $\Phi_{RF}(\varepsilon_{opt};\rho_D^T)$ is the part of the solvent reaction field induced by the donor transition.

Within the TD-DFT approach, the direct coupling is further decomposed into Coulomb (Coul.), Hartree−Fock exchange (HFX), exchange functional (XC), and overlap contributions. The resulting data are presented in Table 6 for the same two structures of $(DMA)_2$ used in the previous section. As a benchmark, the calculations in vacuum are presented as well. In all the results, overlap contributions are virtually zero and are not shown.

Overall, the effects of solvent on the geometry are negligible. This was expected as DTA is a nonpolar system, which cannot strongly interact with a polarizable medium. The effects in the coupling are different in the two $(DMA)_2$ structures. In structure I, the solvent does not modify the Coulomb interaction, but it still slightly modifies the final coupling due to the explicit screening effect. We also tried reoptimization of this structure in THF by DFT/B3LYP with PCM, but the resulting total electronic coupling was 48.1 $cm^{-1}$, which is different from the

(61) Khan, Y. R.; Dykstra, T. E.; Scholes, G. D. *Chem. Phys. Lett.* **2008**, *461*, 305–309.
(62) Knox, R. S.; van Amerongen, H. *J. Phys. Chem. B* **2002**, *106*, 5289–5293.

***Table 6.*** Electronic Coupling (in $cm^{-1}$) for Different Structures of $(DMA)_2$ Calculated by TD-DFT with B3LYP or M06-2X Functional and 6-31+G(d,p) Basis[a]

| | I | | | | II | | | | II′ |
|---|---|---|---|---|---|---|---|---|---|
| | B3LYP | | M06-2X | | B3LYP | | M06-2X | | B3LYP |
| | vac. | THF | vac. | THF | vac. | THF | vac. | THF | vac. |
| Coul. | 54.8 | 54.8 | 75.0 | 74.9 | 82.1 | 105.3 | 108.0 | 137.4 | 53.5 |
| HFX | −1.3 | −1.3 | −5.3 | −5.1 | −0.3 | −0.3 | −0.8 | −0.8 | −0.5 |
| XC | −1.1 | −1.1 | −0.2 | −0.2 | 0.1 | 0.1 | −0.3 | −0.4 | 0.1 |
| PCM | | −4.5 | | −7.3 | | −28.8 | | −37.3 | |
| total | 52.4 | 47.9 | 69.5 | 62.4 | 82.0 | 76.3 | 106.9 | 98.8 | 53.1 |

[a] Both values in a vacuum and in THF solution (calculated by PCM approach) are shown for structures I and II. The value for structure II′ in a vacuum is shown to agree well with the corresponding TDC value.

value shown in Table 6 by less than 1 $cm^{-1}$. In structure II, instead, the presence of the solvent leads to an increase of the Coulomb interactions between D and A, but this increment is almost completely canceled by the screening effect. As a result, the final total coupling does not change significantly from its value in a vacuum. This result seems to indicate that the value of TDC calculation in a vacuum reported in Table 6 is a better estimate of the total electronic coupling than the one divided by $\varepsilon_{opt}$.

By comparing structures I and II (either in a vacuum or in THF), we can also quantify the effects of geometrical distortion from planarity. In the $(DMA)_2$,I structure, which is derived from the real DTA, the two DMAs are no longer planar, and this makes the Coulomb interaction between the two transition densities less effective. This behavior is not reproduced when we define the coupling as one-half the level spacing between states: in that case, the coupling for $(DMA)_2$,I is much larger than that for $(DMA)_2$,II (see Table 6). Also, note the sensitivity of the value to the choice of functional. This indicates possible weakness of direct use of TD-DFT excitation energies for the estimation of electronic coupling in the latter case. In the other case, in the perturbative approach, such weakness is avoided as the transition densities are obtained in the limit of an interaction-free D and A pair. This is clearly an approximation that is valid when the diabatic exciton states in DTA are not significantly different from those where only D or A are excited. Yet at the same time, it also makes the method more stable than the energy-based approach.

**C. Coherent RET (CRET).** While experimental evidence for coherent RET (CRET) dynamics in DTA is convincing, the source of oscillatory behavior with about 1.2 ps period and 1 ps dephasing time is not fully understood. On the other hand, in a semiquantitative theoretical analysis[63] based on a spin-boson model where the major system−bath coupling is assumed to come from the THF solvent with ohmic-type spectral density, it was suggested that such quantum coherence is not plausible. In the present work, we examine this issue based on our theory of CRET[25,26] and a different type of spectral density.

Our theory of CRET[25,26] combines a time-local quantum master equation (QME) formalism[64] with the polaron transformation[65,66] and is applicable beyond the weak system−bath coupling regime. In this theory, the effect of quantum coherence can be assessed directly by comparing the time-dependent population of excitation (diagonal term in the site excitation basis) with that based on the incoherent RET theory.[11] This is in contrast to the measurement of quantum coherence in nonlinear spectroscopy, which typically detects off-diagonal elements of the density matrix in the exciton basis.

Within the effective two-state space spanned by the excited donor and acceptor states $|D\rangle$ and $|A\rangle$, the Hamiltonian governing the RET dynamics can be approximated[11,25,26] by the following spin-boson type Hamiltonian:

$$\begin{aligned} H &= E_D|D\rangle\langle D| + E_A|A\rangle\langle A| + V(|D\rangle\langle A| + |A\rangle\langle D|) \\ &+ \sum_n \hbar\omega_n(b_n + b_n^\dagger)(g_{nD}|D\rangle\langle D| + g_{nA}|A\rangle\langle A|) \\ &+ \sum_n \hbar\omega_n\left(b_n^\dagger b_n + \frac{1}{2}\right) \end{aligned} \tag{7}$$

where $E_D$ and $E_A$ are excitation energies of D and A, $V$ is the electronic coupling between the two, and $b_n$ and $b_n^\dagger$ are lowering and raising operators of the $n$th mode of the bosonic bath approximating all the molecular vibrations and environments. It is assumed that the coupling of exciton states to bath is linear in the displacement of bath coordinates. The parameter $g_{nD}$ ($g_{nA}$) represents the coupling strength of each mode to the excitation of D (A). We introduce two spectral densities $\mathcal{J}_D(\omega)$ and $\mathcal{J}_A(\omega)$ defined as

$$\mathcal{J}_{D(A)}(\omega) \equiv \sum_n \delta(\omega - \omega_n)\omega_n^2 g_{nD(A)}^2 \tag{8}$$

If all the modes are local (coupled to either $|D\rangle$ or $|A\rangle$ only), the above two spectral densities provide complete description of the bath. However, if there exist modes commonly coupled to both $|D\rangle$ and $|A\rangle$, specification of an additional spectral density is necessary.[26] Although common modes can affect the time-dependent behavior of population dynamics significantly,[26] to a large extent, their effects can be accounted for in terms of effective coupling strength within the assumption of local modes only. For this reason, they are neglected in the present work.

Because of the symmetry of DTA, $E_D = E_A$ and $\mathcal{J}_D(\omega) = \mathcal{J}_A(\omega)$. We first assume that the spectral densities have the following super-ohmic form:

$$\mathcal{J}_D(\omega) = \mathcal{J}_A(\omega) = \frac{\eta}{3!}\frac{\omega^3}{\omega_c^2}e^{-\omega/\omega_c} \tag{9}$$

where $\eta$ represents the coupling strength and $\omega_c$ determines the spectral range of the bath. For this spectral density, the reorganization energy $\lambda_{D(A)} = \int_0^\infty d\omega \mathcal{J}_{D(A)}(\omega)\hbar\omega/\omega^2 = \eta\hbar\omega_c/3$. Assuming that this mostly accounts for one-half the difference between the vertical absorption and emission transition energies at zero temperature, which is estimated to be about 1400 $cm^{-1}$ according to Table 2, we can choose $\lambda_D = \lambda_A = 1000$ $cm^{-1}$. For different values of $\omega_c$ under this constraint, the time-dependent population of excited donor $P_D(t)$ was calculated by the full QME in ref 26. For all the cases, it was assumed that $V = 20$ $cm^{-1}$, a small value comparable to that estimated by Yamazaki et al.,[17] and that $T = 300$ K.

Figure 6 shows results for three representative values of $\omega_c/(2\pi c) = 200$, 500, and 1500 $cm^{-1}$. Also compared are time-dependent populations based on the theory of incoherent RET,[11] which we refer to as FRET to imply Förster's RET theory (not necessarily restricted to transition-dipole approximation). The characteristics of coherence are different for each case. The top

(63) Gilmore, J. B.; McKenzie, R. H. *Chem. Phys. Lett.* **2006**, *421*, 266–271.
(64) Jang, S.; Cao, J.; Silbey, R. J. *J. Chem. Phys.* **2002**, *116*, 2705.
(65) Holstein, T. *Ann. Phys.* **1959**, *8*, 343.
(66) Rackovsky, S.; Silbey, R. *Mol. Phys.* **1973**, *25*, 61.

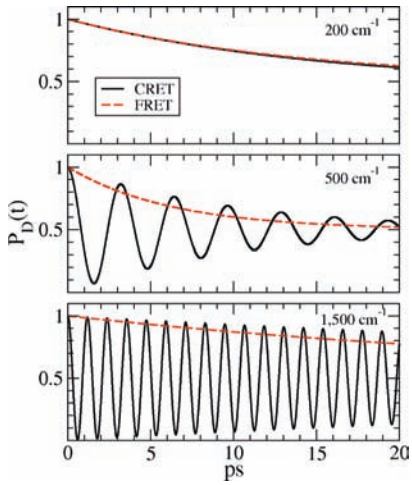


***Figure 6.*** Time-dependent donor population based on CRET and FRET. The top panel is for $\eta = 15$ and $\omega_c/(2\pi c) = 200$ cm$^{-1}$, where $c$ is the speed of light in the cgs unit. The middle panel is for $\eta = 6$ and $\omega_c/(2\pi c) = 500$ cm$^{-1}$. The bottom panel is for $\eta = 2$ and $\omega_c/(2\pi c) = 1500$ cm$^{-1}$. From top to bottom panels, the values of $w$ of eq 11 are 0.0268, 0.259, and 0.704.

panel corresponds to $\omega_c/(2\pi c) = 200$ cm$^{-1}$, where $c$ is the speed of light in the cgs unit. The population dynamics is incoherent from the beginning and agrees almost completely with that of FRET. The middle panel is for $\omega_c/(2\pi c) = 500$ cm$^{-1}$. The coherence is significant and lasts longer than 20 ps, but the period of oscillation is about 3 times that of experimental value. The bottom panel is for $\omega_c/(2\pi c) = 1500$ cm$^{-1}$. The excitation population oscillates with a period of about 1.2 ps. While this is equal to the experimental value,[17] the dephasing is much slower than the experimental estimate of about 1 ps.

The periods of oscillation for the middle and bottom panels of Figure 6 can be understood from the fact that the electronic coupling between the dressed donor and acceptor states formed by the polaron transformation is given by[26]

$$V_{\mathrm{eff}} = wV = \exp\left\{-\int_0^\infty d\omega \coth\left(\frac{\beta\hbar\omega}{2}\right)\frac{\mathcal{J}_D(\omega)+\mathcal{J}_A(\omega)}{2\omega^2}\right\}V \tag{10}$$

where $w$ is the renormalization factor, $\beta = 1/k_BT$, and the second equality shows its general expression in the absence of common modes. For the super-ohmic spectral density, eq 9, this has the following expression:

$$w = \exp\left\{-\frac{\eta}{3!}\int_0^\infty d\omega \coth\left(\frac{\beta\hbar\omega}{2}\right)\frac{\omega}{\omega_c^2}e^{-\omega/\omega_c}\right\} \tag{11}$$

For the two cases shown in the middle and bottom panels of Figure 6, the values of this parameter are 0.259 and 0.704, and the resulting values of $V_{\mathrm{eff}}$ are 5.2 and 14.1 cm$^{-1}$, respectively. These indeed correspond to the oscillation periods of the two results in Figure 6 and show that determination of $V_{\mathrm{eff}}$ only is necessary for the prediction of the period of CRET. Thus, with better choice of spectral density, which produces dephasing rate observed experimentally, it should be possible to deduce the correct value of $V$ from the experimental period of oscillation.

To test whether the super-ohmic spectral density is appropriate, we conducted theoretical calculation of line shapes,[67] which are shown in the left column of Figure 7. Each line shape

(67) Jang, S.; Cao, J.; Silbey, R. J. *J. Phys. Chem. B* **2002**, *106*, 8313.

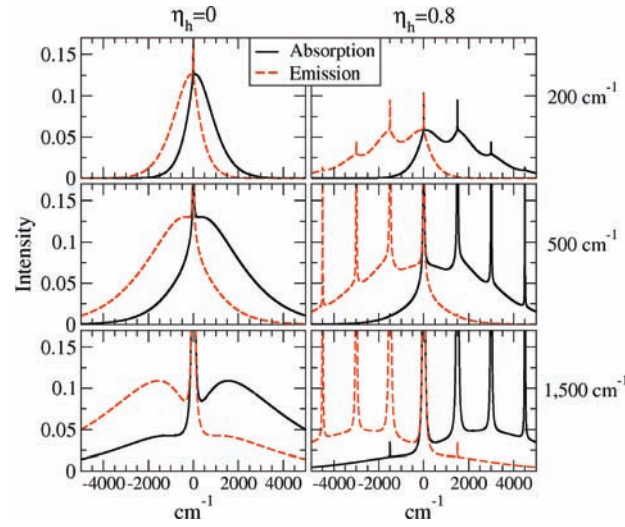


***Figure 7.*** Normalized absorption and emission line shapes. The left column shows line shapes with the super-ohmic spectral density of eq 9 only. The right column shows those with additional high frequency mode, eq 12. From top to bottom panels, $\omega_c/(2\pi c) = 200$, 500, 1500 cm$^{-1}$. A lifetime of 1 ps for the excited state was assumed to ensure fast convergence of numerical integration.

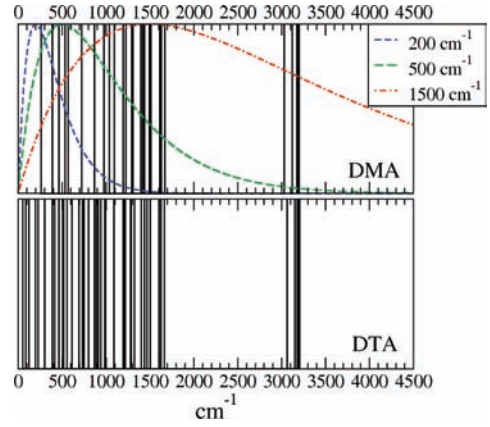


***Figure 8.*** Totally symmetric vibrational frequencies of DMA (upper panel) and DTA (lower panel). In the upper panel, the super-ohmic spectral density divided by $\omega^2$ is shown for different values of $\omega_c/(2\pi c)$. All the spectral densities are normalized with respect to their maximum heights.

consists of a zero phonon line and a vibrational sideband that peaks around $\omega_c$, but none of these produces the vibrational progression of about 1500 cm$^{-1}$ intervals seen experimentally.[17] In Figure 8, the upper panel shows all the frequencies of totally symmetric modes of DMA computed by DFT/B3LYP method with the 6-31+G(d,p) basis for the structure optimized for its ground electronic state. The lowest wavenumber among these is about 264 cm$^{-1}$, and the highest is about 3200 cm$^{-1}$. The mode density of the spectral density, $\mathcal{J}_{D(A)}(\omega)/\omega^2$, for the super-ohmic form eq 9 is also shown for different values of $\omega_c$. The vibrational progression in experimental line shape[17] indicates that the vibrational modes localized around 1500 cm$^{-1}$ in Figure 8 make prominent contributions, which are not captured by the super-ohmic spectral density. As a simple recipe to correct this issue, we tested the following type of spectral density with an additional high frequency mode:

$$\mathcal{J}_{D(A)}(\omega) = \frac{\eta}{3!}\frac{\omega^3}{\omega_c^2}e^{-\omega/\omega_c} + \eta_h\omega^2\delta(\omega-\omega_h) \tag{12}$$

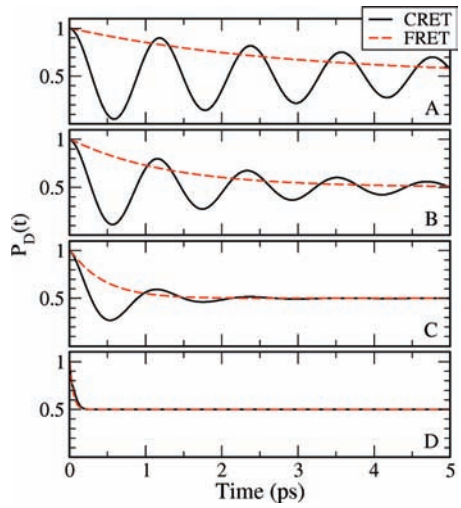


***Figure 9.*** Time-dependent donor population based on CRET and FRET. (A) $V' = 24$ cm$^{-1}$, $\eta = 2.4$, $\omega_c/(2\pi c) = 500$ cm$^{-1}$; (B) $V' = 30$ cm$^{-1}$, $\eta = 3$, $\omega_c/(2\pi c) = 400$ cm$^{-1}$; (C) $V' = 45$ cm$^{-1}$, $\eta = 4$, $\omega_c/(2\pi c) = 300$ cm$^{-1}$; (D) $V' = 150$ cm$^{-1}$, $\eta = 6$, $\omega_c/(2\pi c) = 200$ cm$^{-1}$, where $c$ is the speed of light in the cgs unit. From cases (A) to (D), the values of $w_l$ are 0.582, 0.472, 0.307, and 0.0935.

where $\omega_h/(2\pi c) = 1500$ cm$^{-1}$. The choice of $\eta_h$ is not definite, but we found $\eta_h = 0.8$ reproduces the pattern of experimental vibrational progression reasonably well. The corresponding reorganization energy due to this high frequency mode is 1200 cm$^{-1}$, which accounts for most of the intramolecular reorganization energy of DMA. The right column of Figure 7 shows the resulting line shapes for different values of $\omega_c$. For each case, the value of $\eta$ was chosen such that the corresponding reorganization energy $\eta\hbar\omega_c/3 = 400$ cm$^{-1}$. This value represents the contributions of remaining vibrational modes and the solvent. All the new line shapes now have proper vibrational progressions. In particular, the results for $\omega_c/(2\pi c) = 200$ and 500 cm$^{-1}$ are of the qualitative nature that may provide good modeling of experimental line shape with additional ensemble averaging. Thus, separate consideration of high frequency mode, as was the case for electron transfer reaction[68] for a similar system, appears to be necessary.

For the spectral density given by eq 12, the renormalization factor $w$ has the following form:

$$w = e^{-\eta_h \coth(\beta\hbar\omega_h/2)} w_l = 0.449 w_l \qquad (13)$$

where $w_l$ is the renormalization factor due to the low frequency super-ohmic spectral density and has the same form as eq 11. Given the parameters of this spectral density, which determines the value of $w_l$, we can determine $V$ such that $V_{eff} = 0.449 w_l V = 13.9$ cm$^{-1}$ corresponding to the period of 1.2 ps. For the dynamics calculation, the high frequency mode needs not be included explicitly because it does not cause significant dephasing. Rather, we include its effect by using $V' = 0.449V$ instead of $V$ in the theory. Figure 9 provides four representative results. Except for the case *D*, all show population oscillation at the same frequency but with different dephasing rates. These demonstrate that CRET is indeed possible for DTA. Considering that the dephasing rate for *A* is slower and that for *C* is faster than the experimental value, we can deduce that $V'$ is in the range of 24−45 cm$^{-1}$. The corresponding value of the bare electronic coupling $V$ is in the range of 53−100 cm$^{-1}$. These estimates are based on purely dynamical consideration but are comparable to that based on quantum chemistry calculations in the previous subsections, which corroborates the validity of our estimate.

**D. Inelastic Effect.** The sulfur bonds in DTA are not rigid, and their motion can cause the distance and relative angle between the two anthracene units to change substantially. An obvious effect of this is the modulation of electronic coupling between the two anthracene units. Yet another effect of quantum mechanical origin might be also important if those motions are quantized.

The lower panel of Figure 8 shows the spectrum of totally symmetric vibrational modes of DTA. Most of these can be approximated as symmetric linear combinations of corresponding local modes of DMA. However, there are five distinctive low frequency modes, with wavenumbers of about 49.9, 86.8, 120.0, 197.2, and 227.8 cm$^{-1}$, which represent mutual motion of the two DMAs and cannot be related to local modes of individual DMAs. Among these, we found 86.8 cm$^{-1}$ corresponds to the relative torsional motion between the two anthracene units, and those with 120.0 and 197 cm$^{-1}$ incur significant change in the distance between them. Considering that these are comparable to the value of electronic coupling and the thermal energy at room temperature, the quantum mechanical inelastic effect as addressed in a recent theory[24] can be significant. In this theory, it was shown that some of the transferring energy can exchange with the quanta of distance and torsional modulation, which requires modification of Förster's spectral overlap expression even when transition dipole approximation might be valid.

Considering that the two anthracene units are nearly perpendicular, the torsional motion is expected to have more significant contribution. We conducted constrained optimization of DTA, where the angle between two short axes in Figure 1 was constrained. The ground state was optimized with the constraints of the angle and $D_2$ symmetry by DFT with B3LYP functional but employing a smaller basis set, 6-31G(d). The excited-state energies were calculated by the TD-DFT method. For each structure of DTA with different torsional angle, the corresponding structure of $(DMA)_2$ was created by embedding them into the structure of DTA and matching the positions of three atoms in each anthracene unit. Coulomb coupling between the DMAs was then calculated on the basis of both the TDC method and the approximation of transition dipole interaction.

The results of calculation are shown in Figure 10 as a function of $\phi_{DA}$, which is the angle between two vectors, one from 6 to 12 and the other from 23 to 30 in Figure 1a. The top panel shows theoretical values of electronic coupling calculated by one-half the difference between $S_3$ and $S_4$ energies, the TDC method, and the transition dipole approximation. The middle panel shows the variation of excitation energies from $S_0$ to $S_3$ and $S_4$ states. The values shown here are larger than those in Table 2 because of the smaller basis set used. Still, these data provide useful information for understanding the trend. Finally, the bottom panel of Figure 10 shows the energy of the ground electronic state.

The results shown in Figure 10 provide important clues about the likelihood of inelastic effects. The change of $\phi_{DA}$ within the range of 89−97° is energetically plausible at room temperature. In this range, the energy of the ground electronic state can be well approximated by a harmonic potential, and the variation of the electronic coupling is nearly linear with respect

(68) Markel, F.; Ferris, N. S.; Gould, I. R.; Myers, A. B. *J. Am. Chem. Soc.* **1992**, *114*, 6208.

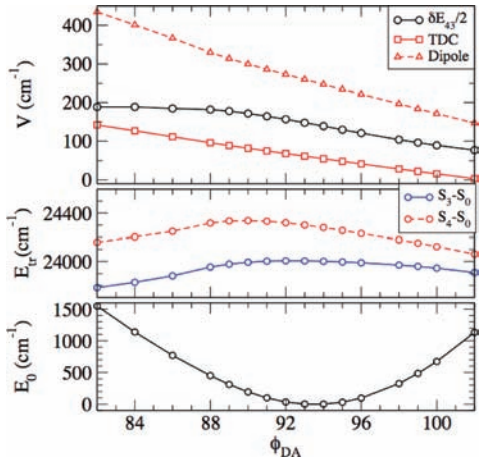


***Figure 10.*** Theoretical values of electronic coupling (top panel) and the energy of ground electronic state (lower panel) as a function of $\phi_{DA}$, the azimuthal angle between the two short axes of anthracene units. The minimum value of $E_0$ in the figure is at $\phi_{DA} = 94°$.

to $\phi_{DA}$. These features are what were assumed in the model Hamiltonian of inelastic FRET[24] and serve as direct evidence for the validity of the model. Thus, it is likely that the kind of inelastic effect addressed in this theory may be active in DTA.

For a more detailed and quantitative understanding of inelastic effect, additional information on the spectral density coupled to the torsional and possibly distance modulation is necessary. This requires simulation of the system with explicit solvent molecules. In addition, considering the importance of quantum coherence, it is necessary to extend the inelastic FRET to the coherent regime. This is possible by applying the formalism of CRET[25,26] to the model Hamiltonian of inelastic FRET. These will be the topics of future study.

## IV. Conclusion

In this Article, we conducted a quantum chemical and dynamical study of the RET process in DTA to understand the nature of electronic excitations, the mechanism of RET process, and quantitative details of coherent RET dynamics.

On the basis of various quantum chemical data, we conclude that the electronic states of DTA probed in experiment indeed correspond to Frenkel-type exciton states at least qualitatively. The value of electronic coupling for $(DMA)_2$,I (in Table 4) is found to be relatively insensitive to a specific method of evaluation and is within the range of about $50-125$ cm$^{-1}$. The electronic coupling of 144 cm$^{-1}$ calculated from TD-DFT/B3LYP excitation energies is somewhat larger than these values, which may contain some errors due to functional (see the Supporting Information for similar estimates based on M06-2X for both structural optimization and excitation energies.). We found that the transition dipole approximation overestimates the actual Coulomb coupling in DTA by at least a factor of 4. Solvent makes a contribution to individual components of the electronic coupling, but the net effect turns out to be relatively minor due to cancellation of polarization and screening effects.

On the basis of the application of the theory of CRET, we conclude that electronic excitations of DTA are coupled to molecular vibrations moderately enough to sustain picosecond time scale electronic coherence. However, the electron−phonon coupling is large enough to cause substantial reduction of the electronic coupling between the donor and the acceptor. In this sense, the value of 20 cm$^{-1}$ as estimated from experiments[17,30] is more representative of such an effective coupling, and the actual bare electronic coupling $V$ is much larger as suggested from our calculation. Our theory of CRET also shows that the value of $V$ larger than 100 cm$^{-1}$ is not plausible because this entails large enough system−bath coupling to make the dynamics incoherent. Thus, combining the results of quantum chemistry and dynamics, we estimate that $V \approx 50-100$ cm$^{-1}$.

While our work resolves many key issues, it also raises other computational and theoretical issues that need more careful examination. Although the TD-DFT/B3LYP approach provided reasonable description of experimental results, we found two dark low-lying singlet states, which appear to be unphysical and need to be understood more clearly. Another issue is to understand how reliable is the electronic coupling constant calculated from the level splitting. Given the accepted errors of TD-DFT in general, the level of agreement shown here is in fact surprising. Is this just coincidental? Or, can it be well justified? Next, is it possible to improve the methodology such that it can serve as a benchmark value? These questions can be addressed through more advanced quantum chemistry calculations. Finally, we explored the possibility of inelastic effect through a series of constraint optimization varying the torsional angle between two anthracene units. The nature of effective potential along the torsional angle and its modulation of electronic coupling are consistent with the model Hamiltonians suggested in a recent theory.[24] Thus, it is possible that the inelastic effect may add another layer of complexity to the coherent RET dynamics in DTA. For a reliable and quantitative understanding of this issue, it is necessary to develop a theory of CRET including the torsional or distance modulation terms. Theoretical work in this direction is currently in progress.

**Acknowledgment.** We thank Brent Krueger for providing the source code of the TDC calculation and valuable comments. We also thank Joe Subotnik and Marshall Newton for helpful suggestions and comments. This work was supported by the National Science Foundation CAREER award (Grant No. CHE-0846899), the PSC-CUNY award (Grant No. PSCREG-62738-0040), the American Chemical Society Petroleum Research Fund (ACS PRF #46735-G6), and the Office of Basic Energy Sciences, Department of Energy (Grant No. DE-SC0001393). S.J. also acknowledges the support of the Dreyfus Foundation through its Camille Dreyfus Teacher Scholar Award.

**Supporting Information Available:** Structural data for DMA, DTA, $(DMA)_2$,I, and $(DMA)_2$,II, and additional data for excitation energies/electronic couplings. Complete refs 49 and 60. This material is available free of charge via the Internet at http://pubs.acs.org.

JA103303U